Available online at www.sciencedirect.com
SCIENCE DIRECT
Cement & Concrete Composites 28 (2006) 486–496
Cement & Concrete Composites
www.elsevier.com/locate/cemconcomp

# Estimating residual stress in the restrained ring test under circumferential drying

Jae Heum Moon, Jason Weiss *

*School of Civil Engineering, Purdue University, 1284 Civil Engineering Building, West Lafayette, IN 47907-1284, USA*

Received 14 June 2004; accepted 31 October 2005
Available online 24 February 2006

**Abstract**

The restrained ring test is becoming widely used as a standard test method to assess the potential for early-age cracking in concrete mixtures. Previous research focused on the development of analytical solutions for quantifying residual stress development in restrained ring specimens that either assumed that the ring was thin (i.e., a thin wall approximation) or that the shrinkage was uniform along the radial direction for a thick-walled ring. This paper presents an analytical solution to consider the influence of moisture gradients that occur when a thick-walled ring specimen dries from the outer circumference. Toward this end, the ring that dries from the outer circumference is treated as the superposition of a stress field that is caused by external restraint and a stress field that arises due to differential shrinkage. An analytical expression is presented to estimate the stress components. To assess the suitability of the analytical solution, it was compared with results from a finite element analysis and a reasonably good agreement was observed.


*Keywords:* Residual stress; Restrained shrinkage; Circumferential drying; Cracking ring-test; Moisture profile

## 1. Introduction and background

Cementitious materials change volume in response to moisture variation, temperature variation, and chemical reaction. If restrained, these volumetric changes result in residual stress development that can lead to cracking. The restrained ring test has recently become a popular method to assess a mixture's susceptibility to restrained shrinkage cracking [1–6]. Over the last 80 years researchers have considered various adaptations of the ring test. For example, early work by Carlson and Reading [7] used the ring to qualitatively compare the shrinkage cracking potentials of various cement compositions. Malhotra and Zoldners proposed that a pressurized ring test could be performed as a potential method for assessing the tensile strength of concrete [8]. Swamy and Stavrides suggested a ring test where strain could be measured for assessing the behavior of fiber reinforced concrete [9]. Grzybowski and Shah used the ring test to investigate strain development in plain and fiber reinforced concrete using strain gages on the concrete surface [10] for the calibration of a modeling approach. Kovler combined the passive restraint from the classic ring test with the active approach advocated by Malhotra for the development of a test with an inner core ring that was made from a material with a higher thermal expansion coefficient. In this test Kovler used the ring to apply passive restraint until a specific time at which a tensile load was applied to the concrete ring by introducing a temperature rise in the specimen assembly [11]. Kovler's approach enabled the testing time to be shortened as the temperature rise that was required to cause fracture was related to the potential additional stress capacity of the material. Weiss and Shah used the ring geometry to demonstrate the benefit of a fracture mechanics approach for predicting the geometry dependent failure of the restrained concrete ring [12]. More recently, in an effort to increase the severity of the test, Li and co-workers proposed an elliptical ring to increase the stress concentration provided by the ring [13].

* Corresponding author. Tel.: +1 765 494 2215; fax: +1 765 496 1364.
*E-mail address:* wjweiss@ecn.purdue.edu (J. Weiss).

0958-9465/$ - see front matter © 2006 Elsevier Ltd. All rights reserved.
doi:10.1016/j.cemconcomp.2005.10.008

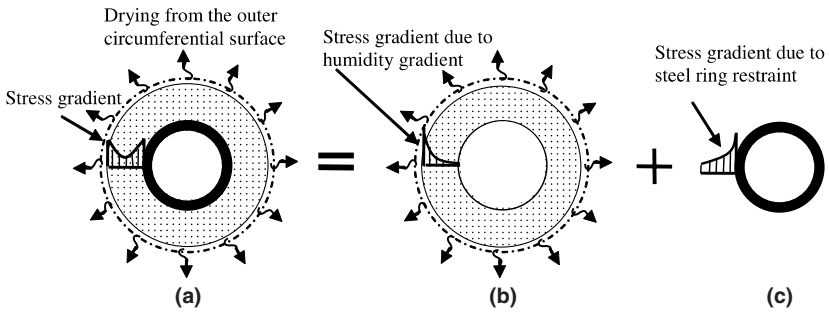


Fig. 1. Conceptual illustration of the restraint components and a sample of stress gradient in the concrete ring. (a) Total stress development, (b) self restraint, (c) ring restraint.

While the aforementioned works show a wide range of applications for the ring approach, this paper builds on recent work to use measurements from an instrumented ring test to make the test more quantitative. Attiogbe and co-workers developed expressions based on a thin ring [14–16] while Weiss and co-workers [17,18] proposed a solution for a thick walled concrete ring under uniform radial drying. This work enabled the strain measured in a steel ring to be used to determine the maximum residual tensile stress in the concrete ring using Eq. (1).

$$\sigma_{\text{Actual-Max}} = -\varepsilon_{\text{Steel}}(t) \cdot E_{\text{S}} \cdot \frac{R_{\text{OS}}^2 + R_{\text{OC}}^2}{R_{\text{OC}}^2 - R_{\text{OS}}^2} \cdot \frac{R_{\text{OS}}^2 - R_{\text{IS}}^2}{2R_{\text{OS}}^2} \tag{1}$$

where $R_{\text{OS}}$ is the outer radius of steel ring, $R_{\text{IS}}$ is the inner radius of steel ring, $R_{\text{OC}}$ is the outer radius of concrete ring, and $E_{\text{S}}$ is the elastic modulus of the steel ring. It should however be noted that although steel was used in this expression the restraining ring can be made of any material provided it remain linear and elastic during the test. It has been subsequently shown that this solution converges with the thin ring solution for a sufficiently small specimen [19]. Additionally, it was shown that the combination of an elastic solution with Eq. (1) can provide an assessment of creep in the ring [20].

While Eq. (1) is appropriate for the case of uniform drying along the radial direction, Fig. 1 illustrates how a moisture gradient develops due to circumferential drying which can significantly influence the stress distribution [12,21–23]. Moisture gradients were described as early as the 1930s by Carlson who began looking at the role of specimen thickness on drying shrinkage [32]. Bazant and Najjar [24] suggested that moisture diffusion analysis could be made more accurate with the use of a diffusion coefficient that was non-linear with moisture content. Bazant and Chern [21] developed a general procedure for considering moisture gradients, stress development and microcracking. Grzybowski and Shah [5,10] developed a model for restrained shrinkage cracking that considered moisture gradients in the ring analysis that used a linear specimen approximation and a continuum damage model while Weiss and Shah [23] used the moisture profile to illustrate the specimen size dependency on the age of cracking. They described how the moisture gradient resulted in complex stress fields that change shape over time [23,25]. To quantify the moisture field that develops Schießl et al. suggested a procedure based on electrical impedance [26]. Grasley and Lange demonstrated a novel sensor [27] which can be used to measure the humidity profile directly. Once the humidity profile is known it can be used to compute the internal residual stress in a specimen [12,27,34]. The existence of moisture gradients has been shown to result in the development of stable surface cracking based on analytical modeling [21,35], acoustic emission measurements [22,39] and optical microscopy [28]. While these papers point toward the importance of moisture gradients in shrinkage and cracking studies, little has been developed in understanding how moisture gradients influence the results that are obtained from the ring test.

The residual stress development and cracking in the restrained ring depends on the drying conditions. Stresses in the thick wall under uniform drying are highest at the inner radius and the stresses decay as a function of $r^2$ [29] while the ring that dries from the outer circumference show that the maximum actual residual stress occurs at the outer radius (at least for short drying times) [23]. This difference in the shape of the stress field is important since it changes how the crack eventually initiates, develops, and propagates. Acoustic emission has been used to show that in rings that dry uniformly along the radius that the cracking begins at the inner circumference of the concrete rings while in specimens that dry from the outer circumference of the rings the cracks begin at the outer edge and propagate toward the center [22,30]. Analytical methods are needed to better characterize the stress field for modeling failure in the ring. This paper outlines a unique approach for determining this stress field by considering the moisture gradient and the steel ring restraint in the analysis of rings that dry from the outer circumference.

## 2. Research significance

This paper describes a solution for determining the residual stress using the restrained ring test geometry in which the residual stress that develops in the ring is thought to be due to a combination of the self-restraint that develops due to non-uniform drying conditions and the restraint

that is provided by the steel ring. Based on this approach, an analytical equation is presented for computing the residual stress field that develops in the restrained ring. This expression can be used to describe stress gradients that develop in a concrete ring. The development of this equation can enable the use of a simple economic test (which has been proposed by AASHTO [2] and more recently under consideration by ASTM [16]) to provide information about the role of moisture gradients in the shrinkage cracking behavior of concrete. In addition to use for standard tests, this approach has implications in predicting the cracking behavior of slabs and bridge decks in which the stress development is due to the concurrent effects of the self-restraint and the restraint by boundary conditions. It is fully anticipated that the approach presented in this paper can be extended for general use in quantifying the cracking potential of concrete under non-uniform drying.

## 3. Analytical approach

It can be argued that the stresses that develop in the restrained ring due to circumferential drying can be considered as a combination of two components as shown in Fig. 1 (i.e., self-restraint due to non-uniform drying and restraint that comes from external restraint supplied by the ring). Therefore, if the residual stress development can be computed for each restraint component, the entire stress field can be obtained.

An example of how the moisture gradient varies in concrete as a function of drying time is shown in Fig. 2 ($\gamma$ is the product of the moisture diffusion coefficient and drying time and is explained in details in the following section) [33]. It can be noticed that for short drying times (i.e., low values of $\gamma$) that the moisture gradient is very severe with the majority of the drying taking place along the outer edge of the specimen. As drying time increases, (i.e., $\gamma$ increases) the depth of the drying front progresses further into the concrete and the moisture distribution is more gradual along the radial direction.

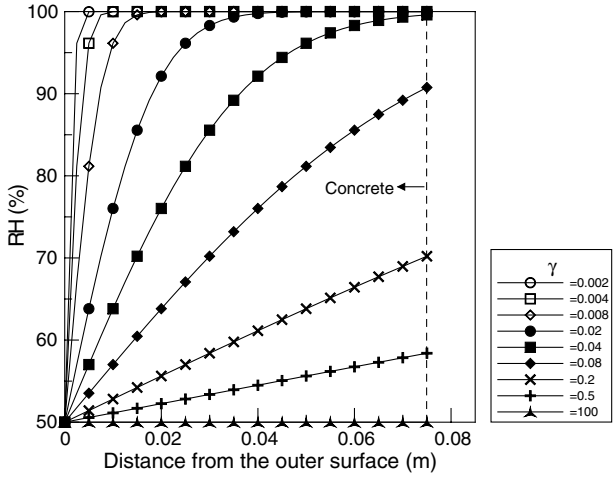


Fig. 2. Relative humidity (RH) gradients calculated using Eq. (3) ($RH_I = 100\%$, $RH_S = 50\%$, thickness = 75 mm).

It should be noted that the loss of moisture causes the specimen to shrink. If the concrete ring is unrestrained (i.e., no steel ring), it will shrink in the radial direction. However, when the steel ring is present, the steel ring limits this shrinkage and residual stresses develop ($\sigma_{\theta\theta,\text{rest.-ring}}$). This restraint causes a pressure to develop at the interface between the steel and concrete which can be calculated directly since the strain at the inner surface of the steel ring (i.e., strain $\varepsilon_{\text{steel}}$) is directly measured [18,31]. In addition to the restraint from the steel, residual stress develops due to self-restraint caused by circumferential drying ($\sigma_{\theta\theta,\text{diff.-shr.}}$). The total stress development can be expressed as the sum of the stress due to restraint and the differential shrinkage.

$$\sigma_{\theta\theta}(r,\gamma) = \sigma_{\theta\theta,\text{rest.-ring}} + \sigma_{\theta\theta,\text{diff.-shr.}} \tag{2}$$

The analytical solution of each component of this expression is further described in Section 5, however in order to enable a better understanding of the foundation of the differential shrinkage behavior due to the moisture gradient, it is first necessary to describe the moisture gradient and its relationship to drying shrinkage in Section 4.

## 4. Moisture gradients and their relationship with shrinkage

The analysis described in this paper considers a ring that is exposed to drying from the outer circumference. The surface that is exposed to drying shrinks more rapidly than the internal concrete which loses water more slowly. Early work on moisture gradients by Carlson in the 1930s considered the moisture gradient to be explained with a diffusion-controlled process similar to that used in thermal analysis [32]. Bazant and Najjar [24] proposed that moisture loss in concrete can be better expressed using a non-linear form of Fick's second law. They proposed that in addition to being age-dependent the diffusion coefficient was non-linear with respect to moisture (i.e., pore pressure, relative humidity, or degree of saturation).

While the non-linear approach is more accurate especially for long term drying, this work will utilize a linear diffusion function (in the form of Eq. (3)) which was fit to physical tests to estimate the humidity profiles as shown in Fig. 2 [33]. The linear diffusion approach is preferred in this paper since it enables the use of the closed-form solution for determining the relative humidity (RH) distribution which is amenable to hand calculation. As a result, a simple moisture gradient can be determined using Eq. (3).

$$\text{RH}(x,t) = \text{RH}_\text{I} - (\text{RH}_\text{I} - \text{RH}_\text{S}) \cdot \left[\text{erfc}\left[\frac{x}{2\sqrt{D \cdot t}}\right]\right] \tag{3}$$

where, $\text{RH}(x,t)$ is the relative humidity at a depth $x$ from the drying surface, $t$ is the drying time, erfc is the complementary error function, $\text{RH}_\text{S}$ is the relative humidity at the surface of the specimen, $\text{RH}_\text{I}$ is the internal relative humidity, and $D$ is the aging moisture diffusion coefficient of concrete. To simplify the combined treatment of the diffusion

coefficient and drying time in this paper, a single parameter ($\gamma$) was introduced as twice the square root of the product of the diffusion coefficient and time ($\gamma = 2\sqrt{Dt}$).

The internal relative humidity (i.e., pore pressure) could be used to predict the induced drying shrinkage strain [34]. The relationship between shrinkage and relative humidity can be approximated for the case of high relative humidity (i.e., RH > 50%) as linearly proportional [12]. As a result, the drying shrinkage strain can be expressed by a constant free shrinkage coefficient ($\varepsilon_{\text{SH-const}}$) and the change of relative humidity ΔRH as illustrated in Eq. (4):

$$\varepsilon(t) = \varepsilon_{\text{SH-const}} \cdot \Delta\text{RH} \tag{4}$$

The constant free shrinkage coefficient ($\varepsilon_{\text{SH-const}}$) can be considered as the slope of the shrinkage versus change in relative humidity relationship. The change of relative humidity (ΔRH) represents the difference between 100% RH and the internal relative humidity RH of a concrete specimen with time.

## 5. Analytical solution

As previously described, the stress development in the concrete ring is mainly due to two components; self-restraint due to differential shrinkage caused by moisture gradients and external restraint due to the effect of the steel ring. In this section, an analytical solution for calculating each component is presented. It should be noted that in its initial form of this solution it is assumed that the concrete ring specimen exhibits linear creep (relaxation) without microcracking [21,22,28,35].

### 5.1. Stress development in the concrete ring due to differential shrinkage: $\sigma_{\theta\theta,\text{diff.-shr.}}(r,\gamma)$

The equation for calculating stress development in the concrete ring due to differential shrinkage can be obtained by using an approach that is similar to the approach used for differential thermal effects [36,37]. It should be remembered that the analysis of the effect of self-restraint does not consider external restraint by the steel ring. Plane stress is assumed in the derivation and due to the axisymmetric geometry the shearing stress at the interface is zero. Using Hooke's law and the drying shrinkage strain from Eq. (4), the stress components (i.e., stress in radial direction: $\sigma_{rr}$ and stress in circumferential direction: $\sigma_{\theta\theta}$) can be expressed in radial components as

$$\sigma_{rr} = \frac{E_{\text{con}}}{1-\nu^2}\left[\frac{\mathrm{d}u}{\mathrm{d}r} + \nu\frac{u}{r} - (1+\nu)\varepsilon_{\text{SH-const}} \cdot \Delta\text{RH}\right] \tag{5}$$

$$\sigma_{\theta\theta} = \frac{E_{\text{con}}}{1-\nu^2}\left[\frac{u}{r} + \nu\frac{\mathrm{d}u}{\mathrm{d}r} - (1+\nu)\varepsilon_{\text{SH-const}} \cdot \Delta\text{RH}\right] \tag{6}$$

where, $u$ is the radial displacement ($\varepsilon_{rr} = \mathrm{d}u/\mathrm{d}r$, $\varepsilon_{\theta\theta} = u/r$), $r$ is the radial distance in the cylindrical coordinates system, and $E_{\text{con}}$ is the effective elastic modulus of concrete (note: the effective modulus can be used to consider the effects of creep). Substituting Eqs. (5) and (6) into the equilibrium equation ($\partial\sigma_{rr}/\partial r + (\sigma_{rr} - \sigma_{\theta\theta})/r = 0$) [36] results in the following expression:

$$\frac{\mathrm{d}}{\mathrm{d}r}\left[\frac{1}{r}\frac{\mathrm{d}(r\cdot u)}{\mathrm{d}r}\right] = \varepsilon_{\text{SH-const}} \cdot (1+\nu)\frac{\mathrm{d}(\Delta\text{RH})}{\mathrm{d}r} \tag{7}$$

This expression can be solved to yield the general solution for the hollow ring geometry:

$$u(r) = \frac{(1+\nu)\varepsilon_{\text{SH-const}}}{r}\int_{R_{\text{IC}}}^{r} \Delta\text{RH} \cdot r\,\mathrm{d}r + C_1 \cdot r + \frac{C_2}{r} \tag{8}$$

where $C_1$ and $C_2$ are constants of integration. Application of the boundary conditions (i.e., no traction on the inner or outer surface of the ring) enables the constants of integration ($C_1$ and $C_2$) to be obtained. Combining Eqs. (5), (6) and (8) enables the residual stress ($\sigma_{\theta\theta,\text{diff.-shr.}}(r,\gamma)$) in the concrete ring caused by differential shrinkage to be computed using Eqs. (9):

$$\sigma_{\theta\theta,\text{diff.-shr.}} = \frac{\varepsilon_{\text{SH-const}} \cdot E_{\text{con}}}{r^2}\left[\frac{r^2 + R_{\text{IC}}^2}{R_{\text{OC}}^2 - R_{\text{IC}}^2}\int_{R_{\text{IC}}}^{R_{\text{OC}}} \text{erfc}(A) \cdot r \cdot \mathrm{d}r + \int_{R_{\text{IC}}}^{r} \text{erfc}(A) \cdot r \cdot \mathrm{d}r - \text{erfc}(A) \cdot r^2\right] \tag{9-a}$$

where, $A$ is given as

$$A = (R_{\text{OC}} - r)/\gamma \tag{9-b}$$

While Eq. (9-a) provides an expression for stress which can be integrated to yield Eq. (10) as a closed-form expression for the residual stress caused by different shrinkage.

$$\sigma_{\theta\theta,\text{diff.-shr.}} = \frac{\varepsilon_{\text{SH-const}} \cdot E_{\text{con}}}{r^2}\left[\frac{r^2 + R_{\text{IC}}^2}{R_{\text{OC}}^2 - R_{\text{IC}}^2} \cdot [f(R_{\text{OC}}) - f(R_{\text{IC}})] + f(r) - f(R_{\text{IC}}) - \text{erfc}(A) \cdot r^2\right] \tag{10-a}$$

where,

$$f(r) = \gamma^2 \cdot \left[\frac{1}{2}\text{erfc}(A) \cdot A^2 + \text{erfc}(A) \cdot \frac{R_{\text{OC}}}{\gamma} \cdot A + \frac{2}{\sqrt{\pi}} \cdot \left(\frac{-A}{4 \cdot \mathrm{e}^{A^2}} + \frac{\sqrt{\pi} \cdot \text{erfc}(A)}{8} + \frac{R_{\text{OC}}}{2 \cdot \mathrm{e}^{A^2} \cdot \gamma}\right)\right] \tag{10-b}$$

The detailed procedures of equation development can be found in Ref. [38].

Fig. 3 shows the example of resulting stress gradients in a concrete ring using Eq. (10) for the case of a ring without steel restraint ($R_{\text{OC}} = 225$ mm, $R_{\text{IC}} = 150$ mm, $\varepsilon_{\text{SH-const}} = -100$ με). The stresses that are developed due to self-restraint have steep gradients near the outer surface when drying begins (i.e., low values of $\gamma$). With increasing drying time (i.e., increasing $\gamma$), the gradient flattens and the shrinkage becomes more uniform. Decreasing the severity of the humidity profile implies that the strain (or stress) developed by self-restraint will be decreased.

### 5.2. Stress development in the concrete ring due to steel ring constraint: $\sigma_{\theta\theta,\text{rest.-ring}}(r)$

The stress development due to the external restraint from the steel ring must also be considered. Previous

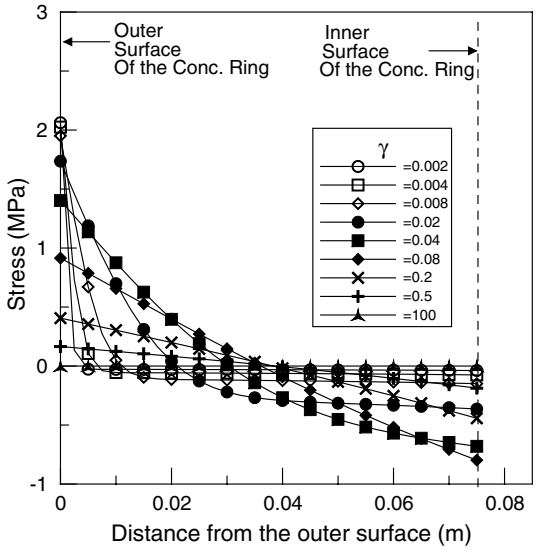


Fig. 3. Stress gradient due to self-restraint in the concrete ring (i.e., without the steel ring (Eq. (10))) ($R_{OC} = 0.225$ m, $R_{IC} = 0.150$ m, $E_{con} = 21$ GPa, $\varepsilon_{SH\text{-}const} = -100$ με).

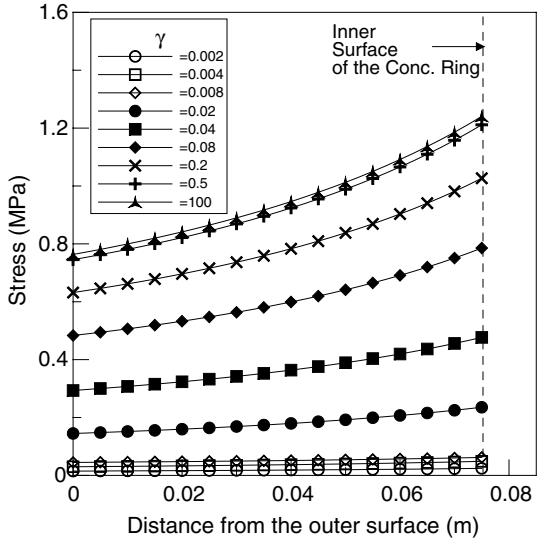


Fig. 5. Stress gradient due to steel ring constraint in the concrete ring (Eq. (12)) ($R_{OC} = 0.225$ m, $R_{IC} = R_{OS} = 0.150$ m, $R_{IS} = 0.1406$ m, $E_{con} = 21$ GPa, $E_{steel} = 200$ GPa, $\varepsilon_{SH\text{-}const} = -100$ με).

research has shown that the restraint from the steel ring can be simulated by separating the steel and concrete ring and treating the problem as a 'shrink-fit' problem. The concrete ring is permitted to shrink by an amount ($\Delta U_{SH}$) that is equal to that caused by drying and autogenous shrinkage. The composite cylinder can be considered to have a fictitious pressure that is applied on the outer surface of the steel ring that is equal to the pressure on the internal surface of the concrete ring [12,17,18,30]. The pressure is adjusted until the steel ring is compressed ($\Delta U_{Steel}$) and the concrete ring is expanded ($\Delta U_{conc}$) to compensate for the shrinkage as shown in Fig. 4 (further details are provided in [18]). The fictitious external pressure could be determined from Eq. (11) since the strain in the steel can be obtained experimentally using the strain gage on the inner surface of the steel ring [18].

$$p_i = -\varepsilon_{steel}(t) \cdot E_S \cdot \frac{R_{OS}^2 - R_{IS}^2}{2 \cdot R_{OS}^2} \tag{11}$$

The fictitious pressure that can be thought to act on the steel ring could be related to an internal fictitious pressure

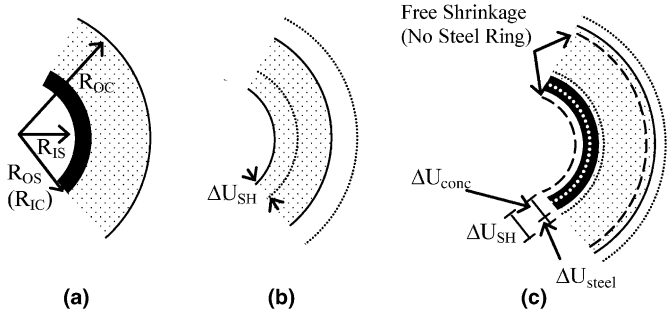


Fig. 4. Conceptual illustration of the 'shrink-fit' approach. (a) Before shrinkage occurs, (b) free shrinkage (no steel ring), (c) shrinkage with steel ring.

that acts on the concrete ring and as a result the stress distribution in the concrete ring can be determined as shown in Eq. (12) [18].

$$\sigma_{\theta\theta,\text{rest.-ring}}(r) = p_i \cdot \frac{R_{OS}^2}{R_{OC}^2 - R_{OS}^2}\left[1 + \frac{R_{OC}^2}{r^2}\right] \tag{12}$$

Fig. 5 shows an example of the stress gradient in the concrete ring calculated using Eq. (12) for the case of the steel ring restraint ($R_{OC} = 225$ mm, $R_{OS} = R_{IC} = 150$ mm, $R_{IS} = 140.6$ mm, $E_{steel} = 200$ GPa, $\varepsilon_{SH\text{-}const} = -100$ με) where $\varepsilon_{steel}$ is the strain that would be measured in the steel ring. The maximum stress develops in the circumferential direction along the interface between concrete and steel. It can be noticed that Eq. (12) is also able to be used in the case of autogenous shrinkage because it can consider a uniform shrinkage of the matrix.

### 5.3. Superposition of differential shrinkage and steel ring restraint

By combining Eqs. (10)–(12), the stress development in the concrete ring can be expressed as the sum of the stress caused by the self-restraint (i.e., differential shrinkage in Section 5.1) and the external restraint (i.e., stress caused by the steel ring in Section 5.2). Eq. (13) enables the stress ($\sigma_{\theta\theta}$) at any point in the concrete ring to be calculated.

$$\begin{aligned}\sigma_{\theta\theta}(r,\gamma) &= \sigma_{\theta\theta,\text{rest.-ring}} + \sigma_{\theta\theta,\text{diff.-shr.}} \\ &= -\varepsilon_{steel}(t) \cdot E_S \cdot \frac{R_{OS}^2 - R_{IS}^2}{2 \cdot (R_{OC}^2 - R_{OS}^2)}\left(1 + \frac{R_{OC}^2}{r^2}\right) \\ &\quad + \frac{\varepsilon_{SH\text{-}const} \cdot E_{con}}{r^2}\left[\frac{r^2 + R_{IC}^2}{R_{OC}^2 - R_{IC}^2} \cdot (f(R_{OC}) - f(R_{IC})) \right. \\ &\quad \left. + f(r) - f(R_{IC}) - \text{erfc}(A) \cdot r^2\right]\end{aligned} \tag{13}$$

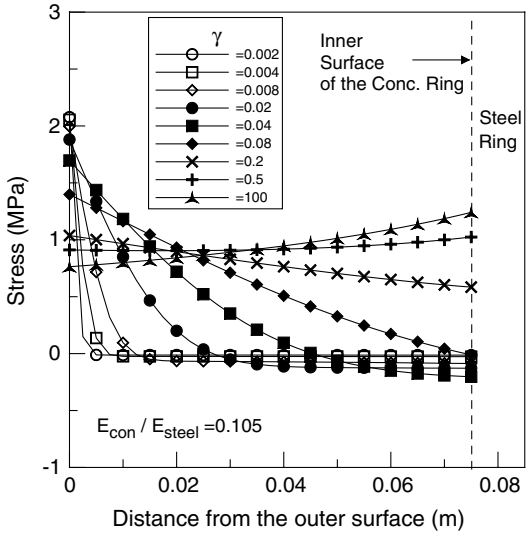


Fig. 6. Stress gradient in the concrete ring exposed to circumferential drying with steel ring (Eq. (13)) ($R_{OC} = 0.225$ m, $R_{IC} = R_{OS} = 0.150$ m, $R_{IS} = 0.1406$ m, $E_{con} = 21$ GPa, $E_{steel} = 200$ GPa, $\varepsilon_{SH\text{-}const} = -100$ με).

Fig. 6 shows the total stress gradient in the concrete calculated using Eq. (13) where the concrete ring is restrained by a steel ring ($R_{OC} = 225$ mm, $R_{OS} = R_{IC} = 150$ mm, $R_{IS} = 140.6$ mm, $E_{steel} = 200$ GPa, $E_{con} = 21$ GPa, $\varepsilon_{SH\text{-}const} = -100$ με). As expected, the stress development is dependent on the extent of drying time (i.e., $\gamma$). It can be noticed that at short drying times the maximum stress occurs on the outer circumference. As drying continues, the position of $\sigma_{Actual\text{-}Max}$ changes from the outer circumference of the concrete ring to the inner surface after $\gamma$ exceeds approximately 0.2 (i.e., longer drying time depending on the elastic modulus of the concrete) (Fig. 6). This can be explained by the fact that, at initial drying times $\gamma$, the stress development in a concrete ring is mainly governed by self restraint, while it is mainly governed by the external steel ring restraint for longer drying periods.

To verify the applicability of the superposition of stresses obtained from Eqs. (10) and (12), each case of restraint (self restraint: Eq. (10) and steel ring restraint: Eq. (12)) will be compared with the results of finite element analysis separately, and Eq. (13) will be finally compared with the finite element analysis in the following section.

## 6. Finite element analysis (FEA)

A series of finite element analyses were simulated using finite element analysis (FEA) in ANSYS to verify the appropriateness of the developed approach. The ring specimen was considered as an axisymmetric geometry where the drying shrinkage gradient occurs along a radial section of the ring specimen. Quadrilateral eight node elements were used for the simulations. The geometry of the concrete specimens simulated in this paper had a depth of 75 mm, an outer radius of concrete 225 mm, and an inner radius of concrete 150 mm. The geometry and material properties of the steel ring were fixed (thickness = 9.4 mm, $E_S = 200$ GPa, and $\nu_S = 0.3$). Poisson's ratio and the effective elastic modulus of concrete were selected to be 0.18 and 21 GPa, respectively. To verify the effect of self-restraint and steel ring restraint, two types of analyses were performed: with the steel ring and without the steel ring.

For the analysis presented in this paper it was assumed that the concrete ring dries only from the outer circumference of the ring. Eq. (3) was used to determine the relative humidity profile while $RH_I$ and $RH_S$ were assumed as 100% RH and 50% RH, respectively. A free shrinkage strain constant ($\varepsilon_{SH\text{-}const}$) was assumed to have a value of $-100$ με.

Finite element analyses were performed by varying the severity of the drying $\gamma$ ($\gamma = 0.001$–100). Theoretically, an infinite value of $\gamma$ corresponds to a concrete ring which dries uniformly along the radius (as described in Eq. (1)), however a $\gamma$ value of 100 was found to be essentially equivalent to higher values, and as such it is the largest $\gamma$ simulated.

Because the FEA program does not support the drying shrinkage loading directly, shrinkage was introduced using a temperature load variable substitution. The temperature distribution was assumed to vary as an error function (erf) (for the sake of this paper, the change in temperature is analogous to a change in relative humidity) and a thermal expansion coefficient was input for the concrete (this can be thought of as being analogous to the free shrinkage constant) to obtain the same effect as drying shrinkage. The maximum stress was selected along a plane perpendicular to the depth direction at midheight in the ring specimen to obtain the stress values that were reported.

The contact condition between steel and concrete for the FE analysis was chosen to simulate an unbonded condition by using a pseudo-bar that essentially permitted a friction free condition along the vertical direction of the ring. This is compatible with the results previously presented in the literature [33].

## 7. Comparison of the analytical approach with FEA and application to an experiment

### 7.1. Comparison with FEA

To verify the appropriateness of the equations that were developed, the stress values calculated by Eqs. (10), (12), and (13) were compared with those obtained from finite element analyses. Fig. 7 shows the stress gradients in the concrete ring without the steel ring restraint as compared to the solution presented in Eq. (10). A generally good agreement was found resulting in minor differences (below 5%) between the finite element analysis and the analytical solution (Eq. (10)) especially for low $\gamma$ values (i.e., short drying times) along the outer circumference of the ring.

To explain some of the differences along the outer circumference of the ring, it should be remembered that the analytical solutions (Eqs. (10), (12), and (13)) were

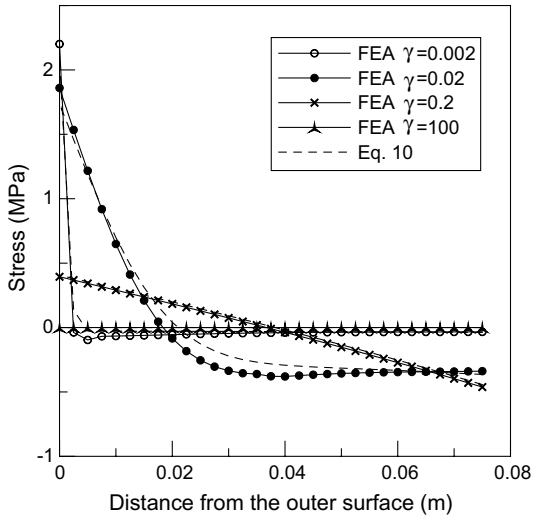


Fig. 7. Comparison of stress gradients due to self-restraint in the concrete ring without steel ring (FEA and Eq. (10)) ($R_{OC} = 0.225$ m, $R_{IC} = 0.150$ m, $E_{con} = 21$ GPa, $\varepsilon_{SH\text{-}const} = -100$ με).

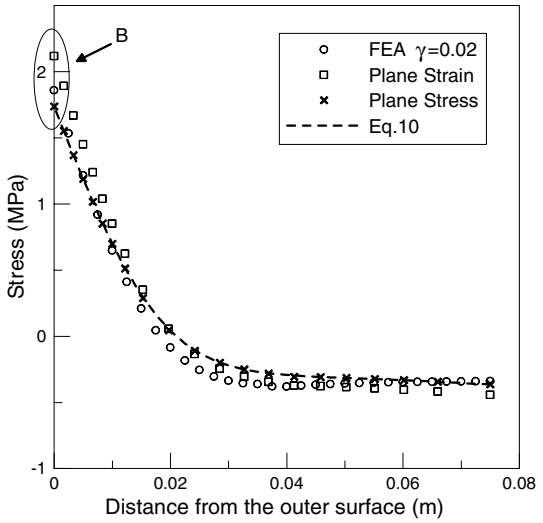


Fig. 9. Comparison of stress gradients due to self-restraint in the concrete ring without steel ring (FEA and Eq. (10)) ($\gamma = 0.02$) ($R_{OC} = 0.225$ m, $R_{IC} = 0.150$ m, $E_{con} = 21$ GPa, $\varepsilon_{SH\text{-}const} = -100$ με).

developed considering plane stress conditions with a uniform stress field in the $z$ (depth) direction. Some of these differences occur due to the plane stress assumption which is not especially well suited for very, very short drying times. To verify this, additional finite element simulations were performed using both plane stress and plane strain conditions. Figs. 8 and 9 show the stress gradients in the concrete ring obtained from the plane stress and strain analysis assuming a uniform stress field in the $z$-direction. As expected the residual stress ($\sigma_{Actual\text{-}Max}$) that was obtained directly from finite element analysis of the actual geometry is located between the plane strain and plane stress approximations (Fig. 10). Since Eq. (10) was developed from the plane stress condition, the values from Eq.

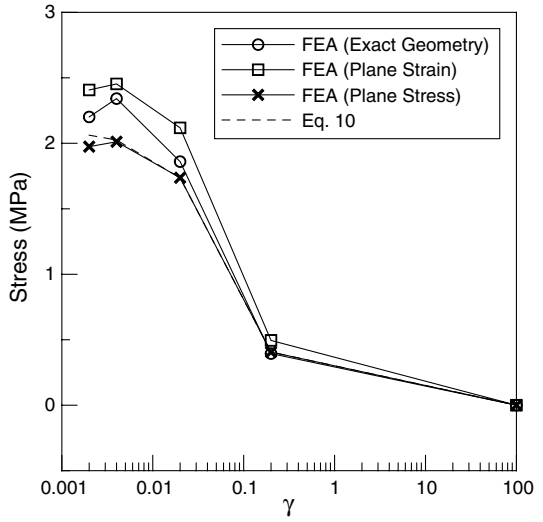


Fig. 10. Comparison of $\sigma_{Actual\text{-}Max}$ due to self-restraint in the concrete ring without steel ring ($R_{OC} = 0.225$ m, $R_{IC} = 0.150$ m, $R_{IS} = 0.1406$ m, $E_{con} = 21$ GPa, $\varepsilon_{SH\text{-}const} = -100$ με).

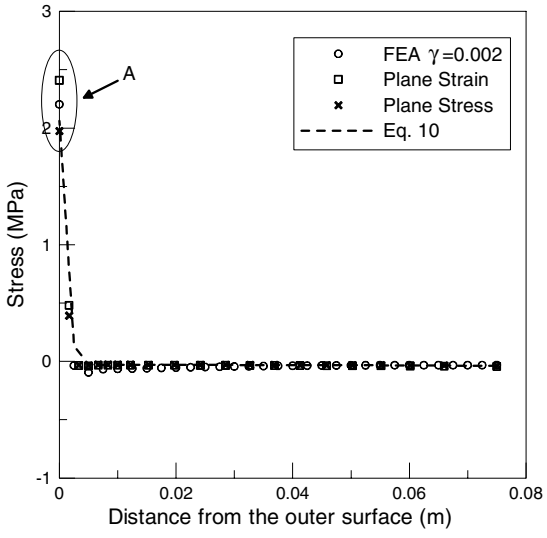


Fig. 8. Comparison of stress gradients due to self-restraint in the concrete ring without steel ring (FEA and Eq. (10)) ($\gamma = 0.002$) ($R_{OC} = 0.225$ m, $R_{IC} = 0.150$ m, $E_{con} = 21$ GPa, $\varepsilon_{SH\text{-}const} = -100$ με).

(10) matched well with those from the plane stress condition finite element analyses (Fig. 10). The results converge toward the plane stress solution as $\gamma$ increases (Fig. 10). It is believed that for a first approximation that this approach is reasonably accurate since it should be remembered that there is a high degree of uncertainty associated with the actual ring specimen tests in which microcracking occurs along the outer circumference.

Fig. 11 shows the stress gradients that developed as a result of the steel ring restraint. The strain values ($\varepsilon_{steel}(t)$) obtained from the finite element analyses were used for the calculations of stress using Eq. (12) and it can be seen that the stress gradients calculated by Eq. (12) corresponded well with those of finite element analyses.

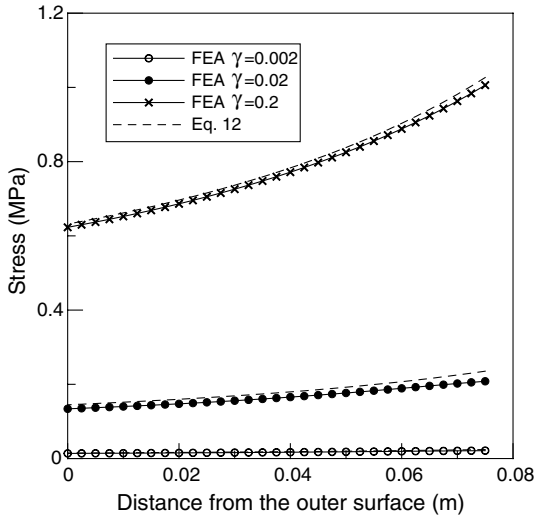


Fig. 11. Comparison of stress gradients due to steel ring restraint in the concrete ring (FEA and Eq. (12)) ($R_{OC} = 0.225$ m, $R_{IC} = R_{OS} = 0.150$ m, $R_{IS} = 0.1406$ m, $E_{con} = 21$ GPa, $E_{steel} = 200$ GPa, $\varepsilon_{SH\text{-}const} = -100$ με).

Since each component of stress development (self-restraint and steel ring restraint) from the analytical solution was separately evaluated, the stress gradients calculated using Eq. (13) (the sum of Eq. (10) (self restraint) and Eq. (12) (steel ring restraint)) were compared with the finite element analyses and a reasonably good agreement was also observed (Fig. 12). As a result, it appears appropriate to utilize the analytical approach described in this paper, if the linear diffusion, linear creep and no micro-cracking assumptions are used.

### 7.2. Application to an experiments

To assess whether the values predicted by this approach are logical and of the right order of magnitude Eq. (13) was used to describe a series of experiments that were performed on a mortar with a water to cement ratio of 0.50 and an aggregate volume of 50% [30]. The ring specimen had an outer radius of the concrete which was of 225 mm, an inner radius of the concrete which was 150 mm, and an inner radius of the steel ring which was 140.5 mm ($\nu_S = 0.3$, $E_S = 200$ GPa). The age-dependent diffusion coefficient was determined for this mixture as described in Eq. (14) using electrical conductivity measurements [33,40]

$$D(t) = d_1 + \frac{d_2}{t} (\times 10^{-12}\ \mathrm{m^2/s}) \tag{14}$$

where, $d_1$ had a value of approximately 9.0 and $d_2$ had a value of 112.64 and $t$ is the drying time which is given in days. The age-dependent splitting tensile strength ($f_{sp}$) was measured and found to be described by Eq. (15) [18].

$$f_{sp}(t) = f_\infty \frac{C_4(t - t_0)}{1 + C_4(t - t_0)} \tag{15}$$

where, $C_4$ was the rate constant with a value of 2.45 day$^{-1}$, $t_0$ was the setting time of 0.25 days and $f_\infty$ was the long term strength which had a value of 4.7 MPa.

Before the maximum residual stress $\sigma_{Actual\text{-}Max}$ was calculated using Eq. (13), two additional material properties needed to be estimated. First, the free shrinkage strain constant was estimated from unrestrained free shrinkage tests. It has been previously shown [18] that the free shrinkage displacement ($\Delta U_{SH}$) can be considered as the combination of the autogenous shrinkage displacement in a sealed specimen ($\Delta U_{AUTO}$) and the drying shrinkage displacement ($\Delta U_{DRY}$) Eq. (16).

$$\Delta U_{SH} = \Delta U_{AUTO} + \Delta U_{DRY} \tag{16}$$

Based on the experimental results [25], Eq. (17) was found to describe the autogenous deformation ($\Delta U_{AUTO}$) in an unrestrained sealed specimen as a function of time

$$\Delta U_{AUTO}(t) = R_{IC} \cdot \varepsilon_{AUTO}(t) = R_{IC} \cdot C_1 (t - t_0)^{C_2} \tag{17}$$

where the coefficients $C_1 = -52.83$, $C_2 = 0.59$, and $t_0 = 0.25$ (mortar, 0.5 w/c, 50% sand) correspond well to measurements in a sealed concrete [17]. The drying shrinkage deformation ($\Delta U_{DRY}$) can be obtained using Eq. (18) which was derived by integrating Eq. (8) [30].

$$\Delta U_{DRY}(t) = \frac{2 \cdot \varepsilon_{DRY\text{-}const} \cdot R_{IC}}{R_{OC}^2 - R_{IC}^2} \int_{R_{IC}}^{R_{OC}} \mathrm{erfc}(A) \cdot r \cdot \mathrm{d}r \tag{18}$$

It should be noted that the free shrinkage strain constant ($\varepsilon_{SH\text{-}const}$) in Eq. (8) is renamed in Eq. (18) as the effective drying shrinkage strain constant ($\varepsilon_{DRY\text{-}const}$) to denote that it only considers the drying shrinkage component since the autogenous shrinkage component is already considered using Eq. (18). The effective drying shrinkage constant of $-1200$ με was estimated for this specific concrete and the deformations predicted by Eqs. (17) and (18) were well correlated to physical measurements.

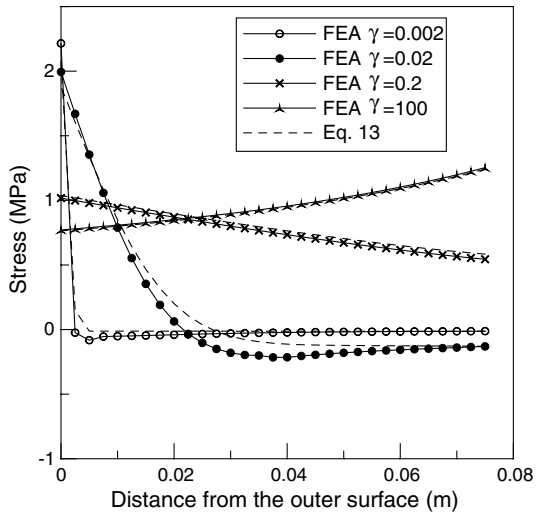


Fig. 12. Comparison of stress gradients due to circumferential drying in a concrete ring with steel ring ($R_{OC} = 0.225$ m, $R_{IC} = R_{OS} = 0.150$ m, $R_{IS} = 0.1406$ m, $E_{con} = 21$ GPa, $E_{steel} = 200$ GPa, $\varepsilon_{SH\text{-}const} = -100$ με).

Second, the effective elastic modulus was estimated using displacement compatibility as illustrated in Fig. 4 [19]

$$E_{\mathrm{con}}(t) = \frac{p_{\mathrm{i}}(t)\cdot R_{\mathrm{IC}}}{\Delta U_{\mathrm{conc}}(t)\cdot (R_{\mathrm{OC}}^2 - R_{\mathrm{IC}}^2)} \times [(1+\nu_{\mathrm{C}})R_{\mathrm{OC}}^2 + (1-\nu_{\mathrm{C}})R_{\mathrm{IC}}^2] \quad (19)$$

where, $p_{\mathrm{i}}(t)$ and $\Delta U_{\mathrm{conc}}(t)$ can be calculated by Eqs. (11) and (16).

With all the material properties now known Eq. (13) was used to compute the stress gradients along the radius of the specimen as shown in Fig. 13. It can be seen in Fig. 13 that almost immediately upon drying the stress that develops on the outer circumference of the concrete ring is higher than the tensile strength. It can be assumed that in the region where the maximum stress exceeds the tensile strength microcracking would occur [21,35,41,25]. It can also be seen that the depth of the concrete in which the maximum stress exceeds the tensile strength increases with time. Fig. 14 shows the progression of stable cracking (i.e., the depth where the residual stress exceeds the tensile strength) in a concrete ring with time thereby suggesting that the crack has propagated at least 8 mm from the surface and this depth of the stable crack is likely greater since these stresses can be expected to be redistributed across the cross-section due to cracking. It should be noted that the laboratory specimen developed a visible crack during the 12th day of drying [30] at which time the magnitude of the average far-field stress is on the order of 2.5–3.0 MPa. If it is assumed that these specimens have properties similar to other mortars ($K_{\mathrm{IC}} \sim 0.5$–$1.0$ MPa mm$^{1/2}$) [43] this far field stress and crack depth could be consistent with the level of stress that is required to cause through cracking.

While this approach appears reasonable, further work is necessary to validate and calibrate this procedure. Specifically, additional work is being performed to enable a description of a wider range of moisture gradients [34,40,27]. Acoustic emission testing is being refined to assess the extent of the stable crack that can be expected to develop from the outer surface of the concrete ring [42] and to document how these cracks develop over time. In addition, further work is being performed to describe how these microcracks coalesce to form a visible crack [28,30].

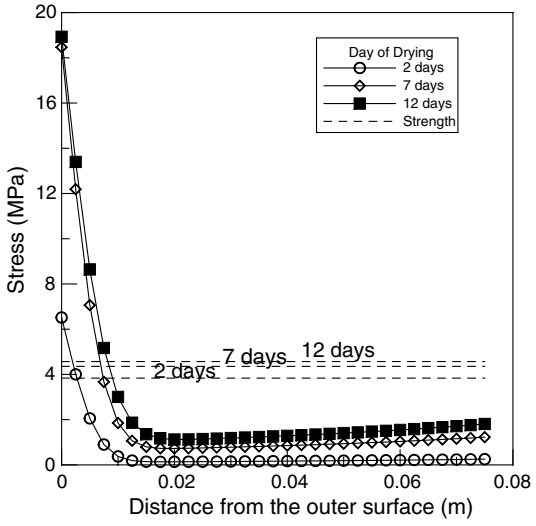


Fig. 13. Stress gradients due to circumferential drying in the concrete ring with steel ring (calculated using Eq. (13) and real test data) (0.50 w/c, 50% sand, $R_{\mathrm{OC}} = 0.225$ m, $R_{\mathrm{IC}} = R_{\mathrm{OS}} = 0.150$ m, $R_{\mathrm{IS}} = 0.1406$ m).

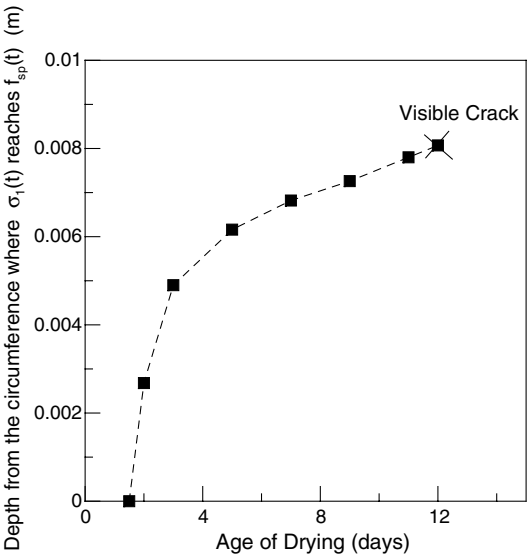


Fig. 14. Predicted depth of cracking in the concrete ring (0.50 w/c, 50% sand, $R_{\mathrm{OC}} = 0.225$ m, $R_{\mathrm{IC}} = R_{\mathrm{OS}} = 0.150$ m, $R_{\mathrm{IS}} = 0.1406$ m).

## 8. Summary and conclusions

This paper has described the development of an analytical approach for calculating stress development in a restrained concrete ring test under circumferential drying. An equation was developed that considered the stress that develops due to restraint by separating the problem into two components: (1) self-restraint due to moisture gradients (Eq. (10)) and (2) external restraint due to the steel ring (Eq. (12)). The analytical residual stress equation (Eq. (13)) was compared with the results from finite element analysis and a reasonable agreement was shown. It was also verified that the restrained ring that dries from the circumference has a high stress at the outer radius for short drying time (i.e., low $\gamma$) and a higher potential to crack from the outer circumference. The developed solutions were applied to properties that correspond to an actual test to show a potential application for the basic approach. This resulted in reasonable stress fields, however further work is needed to demonstrate the application to a wider range of concretes and to improve how relaxation and microcracking are considered.

## Acknowledgments

The authors gratefully acknowledge support received from the National Science Foundation under Grant No. 0134272: a CAREER AWARD granted to the second

author. Any opinions, findings and conclusions or recommendations expressed in this material are those of the author(s) and do not necessarily reflect the views of the National Science Foundation (NSF). This work was conducted in the Charles Pankow Concrete Materials and sensing Laboratories, as such the authors gratefully acknowledge the support which has made this laboratory and its operation possible.

## References

[1] Krause PD, Rogalla EA, Sherman MR, McDonald DB, Osborn AEN, Pfeifer DW. Transverse cracking in newly constructed bridge decks. NCHRP 380, Project 12–37, 1995.
[2] AASHTO PP 34–99, Cracking tendency using a ring specimen.
[3] Shah SP, Karaguler ME, Sarigaphuti M. Effects of shrinkage reducing admixture on restrained shrinkage cracking of concrete. ACI Mater J 1992;89(3):88–90.
[4] Berke NS, Dallaire MC, Hicks MC, Kerkar A. New developments in shrinkage-reducing admixtures. In: Proceedings fifth CANMET/ACI international conference on superplasticizers and other chemical admixtures in concrete, Rome, Italy, 1997.
[5] Grzybowski M. Determination of crack arresting properties of fiber reinforced cementitious composites. PhD thesis, Royal Institute of Technology, Stockholm, Sweden, 1989.
[6] Lim YM, Wu HC, Li VC. Development of flexural composite properties and dry shrinkage behavior of high performance fiber reinforced cementitious composites at early age. J Mater 1999;96(1): 20–6.
[7] Carlson RW, Reading TJ. Model of studying shrinkage cracking in concrete building walls. ACI Struct J 1988;85(4):395–404.
[8] Malhotra VM, Zoldners NG. Comparison of ring-tensile strength of concrete with compressive, flexural, and splitting tensile strengths. J Mater 1967:160–99.
[9] Swamy RN, Stavrides H. Influence of fiber reinforcement on restrained shrinkage cracking. ACI J 1979;76(3):443–60.
[10] Grzybowski M, Shah SP. Model to predict cracking in fiber reinforced concrete due to restrained shrinkage. Mag Concrete Res 1989;41(148):125–35.
[11] Kovler K, Sikuler J, Bentur A. Restrained shrinkage tests of fiber reinforced concrete ring specimens: effect of core thermal expansion. Mater Struct 1993;26:231–7.
[12] Weiss WJ, Shah SP. Restrained shrinkage cracking: the role of shrinkage reducing admixtures and specimen geometry. Mater Struct 2002;35(March):85–91.
[13] He Z, Zhou X, Li Z. New experimental method for studying early-age cracking of cement-based materials. ACI Mater J 2004; 101.
[14] See HT, Attiogbe EK, Miltenberger MA. Shrinkage cracking characteristics of concrete using ring specimens. ACI Mater J 2003; 100(3):239–45.
[15] Attiogbe EK, See HT, Miltenberger MA. Cracking potential of concrete under restrained shrinkage. In: Proceedings, advances in cement and concrete: volume changes, cracking, and durability, engineering conferences international, Copper Mountain, CO, 10–14 August 2003. p. 191–200.
[16] See HT, Attiogbe EK, Miltenberger MA. Potential for restrained shrinkage cracking of concrete and mortar. In: Proceedings of the ASTM symposium on early-age cracking of concrete, December 2003.
[17] Weiss J, Ferguson S. Restrained shrinkage testing: the impact of specimen geometry on quality control testing for material performance assessment. In: Ulm FJ, Bazant ZP, Wittmann FH, editors. Proceedings of the sixth international conference on creep, shrinkage and durability mechanics of concrete and other quasi-brittle materials. Elsevier Science; 2001. p. 645–50.
[18] Hossain AB, Weiss J. Assessing residual stress development and stress relaxation in restrained concrete ring specimens. Cement Concrete Compos 2003;25.
[19] Attiogbe EK, Weiss J, See HT. A look at the rate of stress versus time of cracking relationship observed in the restrained ring test. In: Proceedings of the international RILEM symposium on advances in concrete through science and engineering, March, 2004.
[20] Hossain AB, Shah H, Weiss J. The restrained shrinkage behavior of specimens containing a shrinkage reducing admixture and fiber reinforcement as assessed using the ring test. In: Symposium on assessing early-age cracking of concrete, cement, concrete, and aggregates journal, December 2003.
[21] Bazant ZP, Chern JC. Concrete at variable humidity: constitutive law and mechanisms. Mater Struct, RILEM, Paris 1985;18:1–20.
[22] Kim B, Weiss WJ. Using acoustic emission to quantify damage in restrained fiber reinforced cement mortars. Cement Concrete Res 2003;33(2):207–14.
[23] Weiss WJ, Shah SP. Restrained shrinkage cracking: the role of shrinkage reducing admixtures and specimen geometry. In: Kovler K, Bentur A, editors. RILEM international conference on early-age cracking in cementitious systems (EAC'01), Haifa, Israel, 12–14 March 2001. p. 145–58.
[24] Bazant ZP, Najjar LJ. Drying of concrete as a nonlinear diffusion problem. Cement Concrete Res 1971;1:461–73.
[25] Weiss WJ. Prediction of early-age shrinkage cracking in concrete. PhD dissertation, Northwestern University, August 1999.
[26] Schießl A, Weiss WJ, Shane JD, Berke NS, Mason TO, Shah SP. Assessing the moisture profile of drying concrete using impedance spectroscopy. Concrete Sci Eng 2000;2:106–16.
[27] Grasley ZC, Lange DA. Thermal dilation and internal relative humidity in hardened cement paste. In: Proceedings of the international RILEM symposium on advances in concrete through science and engineering, March 2004.
[28] Bisschop J, van Mier JGM. Shrinkage microcracking in cement-based materials with low water–cement ratio. In: Kovler K, Bentur A, editors. RILEM international conference on early age cracking in cementitious systems, EAC'01, 2001.
[29] Dally JW, Riley WF. Experimental stress analysis. 3rd ed. McGraw-Hill Inc.; 1991.
[30] Hossain AB, Weiss WJ. The role of specimen geometry and boundary conditions on stress development and cracking in the restrained ring test. Cement Concrete Res 2006;36(1):189–99.
[31] Shah HR, Hossain AB, Mazzotta G, Weiss WJ. Time-dependent fracture in restrained concrete: the influence of notches and fibers. In: Proceedings of advances in cement and concrete IX: volume change, cracking and durability, Copper Mountain, Colorado, 2003.
[32] Carlson RW. Drying shrinkage of large concrete members. J Am Concrete Inst 1937(January–February):327–36.
[33] Moon JH, Rajabipour F, Weiss WJ. Incorporating moisture diffusion in the analysis of the restrained ring test. Presentation at CONSEC, Seoul Korea, June 2004. p. 1973–80.
[34] Bazant ZP, editor. Fourth RILEM international symposium on creep and shrinkage of concrete: mathematical modeling. Northwestern University; 1986.
[35] Granger L, Torrenti JM, Acker P. Thoughts about drying shrinkage: experimental results and quantification of structural drying creep. Mater Struct 1997;30:588–98.
[36] Boley BA, Weiner JH. Theory of thermal stress. Dover Publications; 1988.
[37] Timoshenko SP, Goodier JN. Theory of elasticity. McGraw-Hill College Div; 1970.
[38] Moon JH. Shrinkage, residual stress, and cracking in heterogeneous materials. PhD thesis, Purdue University, 2006.
[39] Chariton T, Weiss WJ. Using Acoustic emission to monitor damage development in mortars restrained from volumetric changes. In: Shah Surendra P, Balaguru P, Namaan A, Weiss W, editors. Concrete: material science to application, a tribute to ACI SP-206, p. 205–18.

[40] Rajabipour F, Weiss J, Abraham D. Insitu electrical conductivity measurements to assess moisture and ionic transport in concrete. In: Proceedings of the international RILEM symposium on advances in concrete through science and engineering, March 2004.
[41] Grasley ZC, Lange DA, D'Ambrosia MD. Internal relative humidity and drying stress gradients in concrete. In: Engineering conferences international, Advances in cement and concrete IX, Copper Mountain, CO, 2003. p. 349–63.
[42] Neithalath N, Moon JH, Rajabipour F, Barde A, Weiss J. Attiogbe E. The role of binder composition in early-age shrinkage cracking: modelling how moisture gradients influence time dependent cracking. In: NSF workshop on high performance cementitious composites, Chennai, India, January 2005.
[43] Shah SP, Jenq YS. On the concrete fracture testing method. In: Minashi et al., editors. Fracture toughness and fracture energy. Balkema Publishers; 1989.